ChemPubSoc Europe

DOI: 10.1002/batt.201800068

BATTERIES & SUPERCAPS Communications

Dual-IR Window/Electrode Operando Attenuated Total Reflection-IR Absorption Spectroscopy for Battery Research

Hamed Ataee-Esfahani[+],[a] De-Jun Chen[+],[a] and YuYe J. Tong*[a]

We report a novel dual-IR window/electrode operando infrared (IR) spectroscopy method for battery research. In addition to keeping all the features of the in-situ/operando IR spectroscopic methodologies for batteries reported in the literature so far, the dual-IR window/electrode configuration reported herein offers a unique advantage of accessing both, anode and cathode processes quasi-simultaneously by rotating the dual-window/electrode IR battery cell 180° step-wise in the same operando real-battery-like cell. The proof-of-concept studies demonstrated clearly its investigative advantages in gaining broader insights into the chemistry of batteries during charging/discharging and beyond.

A wide range of current environmental problems that the world faces (including climate change and air pollution) results from persistent use of fossil fuels. In spite of the recent achievements on producing power using renewable sources such as solar and wind energies, the intermittent nature of those green sources makes energy storage systems necessary for their sustainable use. Rechargeable batteries, particularly Li-ion batteries (LIBs), with high mobility and energy density are becoming major energy storage systems.[1–5] In LIBs (or rechargeable batteries in general), conversion between chemical and electrical energy occurs through controlled reversible chemical reactions between a set of active chemicals. These reactions are usually accompanied by unwanted side reactions that consume active materials or impede their reactions. Unraveling the details of the involved chemistries is the key to improve the performance of current batteries or to develop new batteries with better performance. The challenge, however, is that LIBs have to work in an air-tight, oxygen and moisture free environment as the chemical processes at electrodes are air-sensitive and Li-ion-containing organic electrolytes are highly flammable. This dictates that, in order to truly understand the underlying chemistries, many key battery processes have to be studied by in-situ/operando techniques;[6] yet many of the latter are still at an early stage of development, which includes in-situ/operando electrochemical (EChem) infrared (IR) spectroscopy.[7–14] Although most recent in-situ EChem IR studies[8–15] employed attenuated total reflection (ATR) mode to overcome the problem of hindered ionic diffusion caused by the earlier thin-layer mode,[6,7] they also adopted a half-cell configuration against a Li metal electrode and most likely with an in-between-electrode physical dimension that was not commensurate with that of real-world batteries, which leaves room for further improvements. With these observations in mind, we report herein a novel dual-ATR window/electrode configuration that offers a unique advantage of accessing both anode and cathode processes quasi-simultaneously in the same operando real-battery-like cell. The proof-of-concept studies carried out demonstrated clearly its investigative advantages in gaining insights into battery chemistry.

Figure 1 shows the schematic diagram, individual components and their respective physical dimensions of the dual-ATR

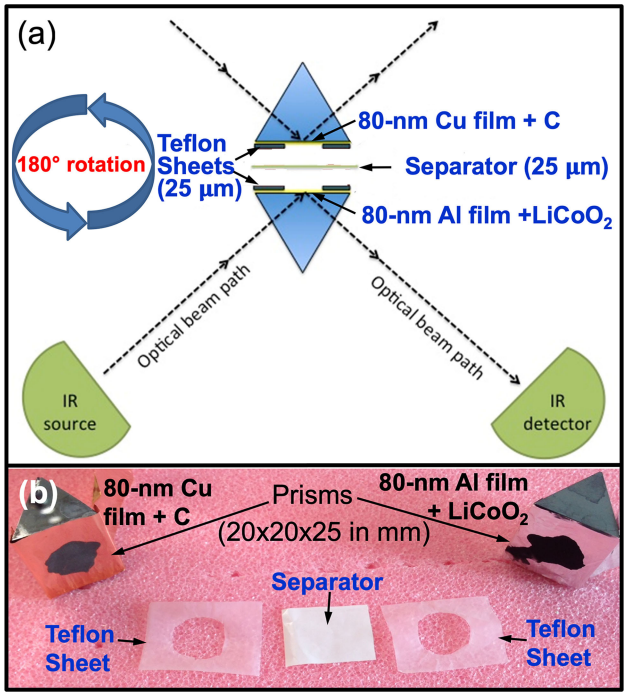

Figure 1. (a) Schematic diagram and (b) individual physical components of the rotating dual-IR window/electrode operando Echem ATR-IR setup. The two prisms were clamped together tightly by which an air-tight, IR accessible functional LIB was formed. During the battery charging or discharging process, the setup was mechanically controlled by a computerized step motor that flipped it 180° step-wise periodically, moving one prism to a fixed position for synchronized sequential IR measurements without interrupting the battery operation.

[a] *Dr. H. Ataee-Esfahani,[+] Dr. D.-J. Chen,[+] Prof. Dr. Y. J. Tong*
Department of Chemistry
Georgetown University
37th & O St, NW, Washington DC, 20057 United States
E-mail: yyt@georgetown.edu
[+] *These authors contributed equally*

Supporting information for this article is available on the WWW under https://doi.org/10.1002/batt.201800068

window/electrode operando IR setup for batteries in which graphite and $LiCoO_2$ were used as active anode and cathode materials respectively for the proof-of-concept measurements. On the one Si prism ATR window, a ~80-nm thick Cu layer was first sputtering-deposited under ultrahigh vacuum that was used as the anodic current collector and served as a protecting layer to prevent Li intercalation into Si prism. Then 10 μL graphite slurry of a well sonicated mixture of graphite powder and N-Methyl-2-pyrrolidone (NMP) in a concentration of 0.2 mg/μL was drop-casted onto the Cu layer. On the other Si prism ATR window, a ~80-nm thick sputtering-deposited Al layer was used as the cathodic current collector. Then 10 μL $LiCoO_2$ slurry of a well sonicated mixture of $LiCoO_2$ powder and NMP in a concentration of 0.4 mg/μL was drop casted onto the Al layer. Both prisms were first dried in a drying oven at 50 °C and then baked in a tubular oven at 110 °C for 4 hours under a controlled Ar atmosphere. The battery cell with a 25-μm thick separator and two 25-μm thick Teflon-sheets with a circular aperture in the center was then assembled immediately in a glove box by clamping the two prisms together tightly after the electrode materials were wetted by an appropriate amount of electrolyte containing 1 M $LiPF_6$ in the mixture of EC (ethyl carbonate):DEC (diethyl carbonate) (1:1 ratio) (Figure 1a). However, one technical challenge that we encountered in the process and needs further improvement in the future was that we did not have a reliable way to assess whether the battery materials surface was fully wetted or not when the electrolyte was injected, which might leave some electrochemically dead surface once the LIB was assembled together. It is also difficult to estimate the exact thickness of the active electrode materials but 5 to 10 μm is a reasonable estimate based on the density, surface area and amount of the material deposited. The assembled operando IR battery cell was then mounted to the shaft of a computerized step motor that could rotate 180° stepwise and moved one prism into a fixed measuring position periodically in a synchronization with the ATR-IR data acquisitions. The latter were carried out on a Cary 670 Fourier transform IR spectrometer equipped with a liquid-nitrogen-cooled mercury-cadmium-telluride (MCT) detector. The spectral resolution was set to 4 cm^{-1}. The stability of IR acquisitions during the rotations was assessed by monitoring the C=O IR band amplitude of DEC as a function of time. As can be seen in Figure S1 (see Supporting Information-SI), the IR amplitude was highly stable except for the less than 2-s period at the moment of prisms rotation. The rate of spectral acquisition was set 0.04 s per spectrum during the LIB charging and discharging. But only the spectra in the time period of 5 seconds before and after a listed potential were averaged to give the one spectrum assigned to that potential. The obtained spectra were shown in the absorbance units defined as $-\log(I/I_0)$ where I and I_0 are the single-beam spectral intensities at the measuring potential and the reference potential, respectively. No baseline subtractions or other post-acquisition spectral treatments were done as the spectral details were cell potential dependent.

The penetration depth of ATR for Si window is ~0.81 μm. But we expected that it would be shorter than that in our case as ~80-nm thick Cu or Al film was deposited onto the Si prism surface. The implication of the limited penetration length is that the ATR-IR can only see a small portion of the battery material if its thickness is much larger than the penetration length, which may legitimately raise concerns about whether or not the battery chemistry in the region that can be investigated by the ATR-IR is the same as that in the region that cannot be seen by the ATR-IR. However, as long as all battery materials can be homogeneously accessed electrochemically, it is reasonable to assume that the battery chemistry in the region that can be investigated by the ATR-IR would also represent well that in the region that cannot be seen by the ATR-IR. As such, ensuring that the battery materials are fully wetted by electrolyte becomes critically important for obtaining reliable and meaningful data. As mentioned above, this is still technical challenge we face.

The as-assembled IR battery cell showed an open circuit potential (OCP) around 0 V at which reference IR single-beam spectra (Figure 2) were recorded for both the anode (red) and cathode (blue). Interestingly, these single beam spectra already showed that the solvent molecules (EC vs. DEC) interacted differently with the anode and cathode at this initial stage. By comparing with the peak positions and relative amplitudes of the reference spectra[16] shown in Figure S2, we assigned the peaks identified by red vertical dashed lines to EC and those by blue lines to DEC. On the $LiCoO_2$ cathode, only DEC was observed. But on the graphite anode, both EC and DEC were observed, which indicates that EC interacted preferentially with anode. The affinity of EC to the graphite surface probably arises from that the positive charge of EC-solvated Li^+ ion is more attracted by the usually negatively charged carbon surface as EC has a higher polarity, 4.9 D, to solvate Li^+. The comparable DEC band amplitudes on the both electrodes imply that the latter has much less if any preference to carbon over $LiCoO_2$.

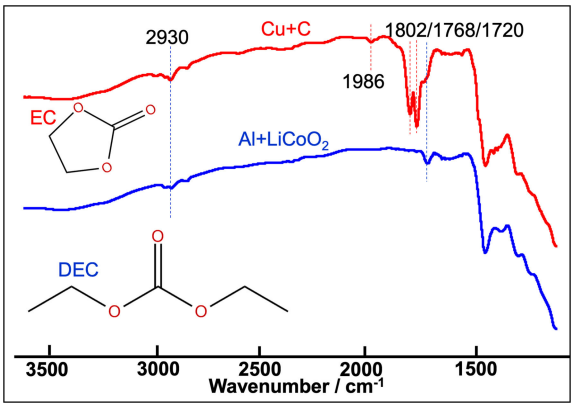

Figure 2. Single-beam operando IR spectra recorded at the anode (red) and cathode (blue) at OCP. Vertical lines indicate peaks assigned to EC and DEC.

Among many key chemical processes that contribute to the ultimate performance of a battery, the formation and stability of the so-called solid-electrolyte interphase (SEI) layers on the electrode surfaces have been a focus of many studies.[17–21] In LIBs, the active anode and cathode materials can usually

accommodate a wide cell potential ranges but the organic solvents and electrolyte components are only stable within certain cell potential ranges and become unstable, i.e., being oxidized or reduced, at either cathode ($LiMO_x$) or anode (graphite) if the battery is overcharged ($E > 4.2$ V) or overdischarged ($E < 2.5$ V).[22,23] In the case of graphite anode, the EChem reduction of electrolyte solution during the battery charging results in the formation of the SEI layer. The stability of the formed SEI layer is dependent on composition and additives. For instance, it was observed that if EC-based materials were used as solvents for electrolyte, the SEI layer remained stable enabling Li intercalation and de-intercalation; but if propylene carbonate (PC) based electrolytes were used, co-intercalation of the solvent molecules and exfoliation of graphite layers were observed.[24–27] Although various electrolyte additives were found to facilitate the formation of a stable SEI layer and prolong the battery life, the underlining chemistry that governs the SEI's impact on the LIB performance is still far from clear.[21,25,28–32] As electrode/electrolyte interfacial compounds are highly air and humidity sensitive, it is highly desirable to study the SEI-related chemistries in operando.

Figure 3 shows the operando EChem ATR-IR spectra for the crucial 1st charge during which the SEI is supposed to form and the subsequent discharge cycle on the graphite/electrolyte interface of the IR battery cell as a function of the charging and discharging process with a rate of 0.1 C. During the charging process from the OCP 0 V to fully charged potential 4.1 V, four positive bands at 1818, 1780, 1736 and 1316 cm^{-1} and one negative band at 1437 cm^{-1} were emerged when battery was charged up to 4.1 V, indicating the formation of the SEI layer. As can be seen in Figure 3b, the formation of SEI initiated at 2.50 V and kept growing until 4.1 V that is characterized by the distinct 3-band SEI structure. Interestingly, the decrease of the band at 1437 cm^{-1} and the formation of the band at 1316 cm^{-1} were correlated with the SEI formation process (Figure 3b). More specifically, the pair of positive bands at 1736 and 1316 cm^{-1} bands can be assigned to the DEDOHC (diethyl 2,5-dioxahexane dicarboxylate) formed inside the SEI layer, similar to what observed on Sn.[16] The other pair of positive bands at 1820 and 1780 cm^{-1}, on the other hand, can be assigned to EC and Li-ion associated EC inside the SEI layer.[9] These SEI IR bands observed herein match those reported in the literature but with slight peak shifts and different shapes and relative peak intensities. The possible reasons for the observed differences are (i) different anode material (graphite vs. Sn), (ii) different ratio of electrolytes (EC:DEC = 1:1 vs. EC:DEC = 1:2), and (iii) different cell configuration (2 electrodes vs. 3 electrodes). As to the negative band at 1437 cm^{-1}, we assigned it to the bending motion of displaced graphite terminal functional group C=C–H[33] by the formation of the SEI layer on the graphite surface. The aforementioned band assignments were listed in Table S1.

At the onset (3.46 V) of the ensuing normal discharging from 4.1 V to 2.52 V (Figure 3a), although the three neighboring SEI bands showed a similar degree of decrease in amplitude, the rightmost one that is assigned to DEDOHC had the largest blue-shift by ~12 cm^{-1}, indicating that it had the strongest interaction with the environment. The latter is consistent with that the rightmost band appeared to be also most unstable (vide infra). Moreover, the 1316 cm^{-1} band already disappeared, which also suggests a breakdown of DEDOHC. After the initial change at 3.46 V, the amplitudes of the three surviving bands remained rather constant, indicating that SEI layer was rather stable during the normal charging process. Over-discharging the battery starting at 2.43 V (Figure 3c) saw an immediate amplitude decrease of the rightmost band at 1747 cm^{-1} (indicated by the vertical red dashed line) and became smaller and smaller as the over-discharging continued. In contrast, the

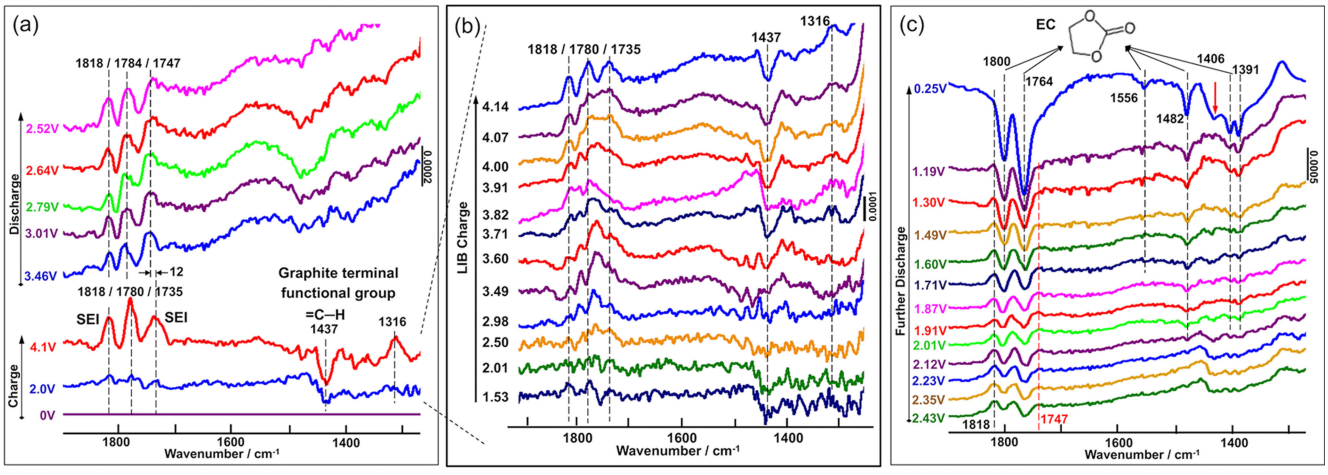

Figure 3. Operando EChem ATR-IR spectra for the 1st charge and discharge cycle on the graphite/electrolyte interface of the IR battery cell: (a) from OCP (0 V) to fully charged potential 4.1 V, which is zoomed in for more details in (b), and then to 2.52 V (normal charge and discharge process) and (c) from 2.43 V to 0.25 V (overdischarge process). Notice that the spectrum at 4.1 V in (a) resulted from a co-add of 250 interferrograms (10 s of signal acquisition) while those in (b) from co-add of 2500 interferrograms (100 s of signal acquisition), which might be the cause of somewhat baseline difference in them. The band indicated by the red arrow in the spectrum at 0.25 V is at 1437 cm^{-1}, which can be assigned to the bending motion of same graphite terminal functional group C=C–H in (a) at 4.1 V. As the spectrum recorded at 0 V was used as a reference spectrum, it appears as a flat line in (a). Thus, the increase or decrease of the band intensity is with respect to the surface situations at the OCP of ~0 V.

amplitudes of the other two bands at 1818 cm^{-1} and 1784 cm^{-1} did not change much until 1.49 V. As the 1747 cm^{-1} band was assigned to DEDOHC which was most likely formed from DEC, the SEI components formed from EC appeared to be more stable than those formed from DEC. Notice that there was a band near 1316 cm^{-1} re-appeared in Figure 3c. Although we are unable to assign it to a definitive species, we speculate that it must come from a species that had a O–C–O vibration of which the frequency happened to be in the region of 1316 cm^{-1}.

Negative growing bands at 1800 cm^{-1} and 1764 cm^{-1} that can be assigned to solvent EC appeared and grown larger and larger as the over-discharging continued from 1.49 V to 0.25 V (Figure 3c), indicating that the carbon anode became more and more repellant to the near-electrode EC, which is also confirmed by the other decreasing smaller bands of EC at low frequencies of 1556, 1482, 1406 and 1391 cm^{-1}. This observed EC repelling is in contrast to the graphite anode's initial affinity toward EC at the OCP (Figure 2), implying a significant change of surface condition (vide supra). While further decomposition of organic solvents and growth and compositional changes of the SEI layer are also expected over this deep overcharging, a clear ATR-IR observing them was masked by the two overwhelmingly large negative going EC bands. But the disappearing of the leftmost band at ~1818 cm^{-1} as indicated by the leftmost dashed vertical line still suggests a continuous disintegration of the SEI layer.

Figure 4 presents the operando ATR IR spectra acquired during the same charging and discharging cycle as in Figure 3 but at the $LiCoO_2$ cathode. The slight potential differences from those in Figure 3 are the result of sequential acquisitions after every 180° flip of the prisms. During the charging to 4.2 V, two bands at 1808 and 1775 cm^{-1} emerged that can be assigned to

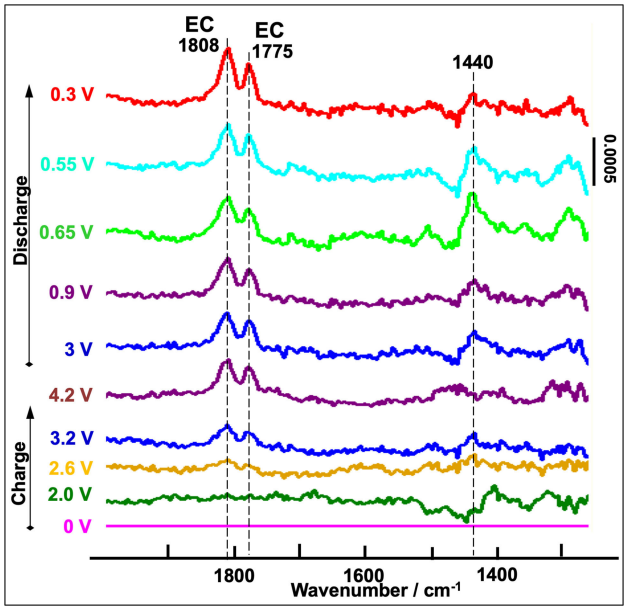

Figure 4. In operando EChem ATR-IR spectra for the 1st charge and discharge cycle on the $LiCoO_2$/ electrolyte interface of the IR battery cell: from OCP (0 V) to fully charged potential 4.2 V then to over-discharged state of 0.3 V.

EC.[9] These two bands were stable during the normal discharging and also over-discharging all the way up to 0.3 V. The increased affinity of $LiCoO_2$ to EC molecules is further confirmed by the appearance of the bands at 1802/1768 cm^{-1} in the single-beam spectrum recorded after the charging/discharging (Figure S3). That no EC bands were observed at the OCP (0 V, Figure 2) strongly suggested that these two bands came from a stable SEI layer on the $LiCoO_2$ cathode that was formed during the first charging process and remained largely stable over the entire ensuing discharging and over-discharging process, in great contrast to the SEI formed on the graphite anode. A band at 1440 cm^{-1} that can be assigned to $\delta(CH_3)$[9] appeared during the discharging process. As it appears to be an unstable band, we tentatively assign it to some CH_3-containing fragment(s) from the breakdown of DEC or/and DEDOHC in the electrolyte.

It is interesting to point out that the negative band of C=C–H at 1437 cm^{-1} observe at fully charged state at 4.1 V (Figure 3a) persisted in the spectrum recorded at lowest over-discharging potential (0.25 V, Figure 3c, indicated by the red arrow at 1435 cm^{-1}). However, over the LIB charging and discharging processes, this negative C=C–H band could also disappear or become smaller: between 2.50 V and 3.60 V during the charge (Figure 3b), 3.64 V and 2.52 V during the normal discharge (Figure 3a), and 2.43 V and 1.19 V during the over-charge (Figure 3c) process, which indicate the complex chemical processes taking place on the carbon surface. As the physical formation of the SEI did not initiate until 2.50 V, the early appearance of the negative band at 1437 cm^{-1} from 1.53 V to 2.01 V (Figure 3b) implies a process different from the physical displacement by the SEI formation. We speculate that this might be that part of the initial intercalating Li-ions were reduced by the surface functional group. As the charging process continued and the formation of SEI initiated, intercalating Li-ions were no longer reduced by the surface functional group which led to their reappearance on the surface. But in the end, the physical displacement by the formed SEI took over. On the other hand, the de-intercalation of Li-ions during the normal discharge and most part of overdischarge period seemed to reverse the process. Finally, the disintegration of the SEI at the lowest cell potential of 0.25 V might cause a significant modification of the carbon surface as implied by the large decrease of surface EC which would prevent a full restoration of the initial surface C=C–H groups. Such an irreversible carbon surface modification after a full cycle of charging and over-discharging process might also be related to the decay of LIB cycle life.

Equally interesting is that in the same spectrum, an increase of a band at 3268 cm^{-1}, which can be assigned to ν(OH) on the graphite surface,[34] was observed (Figure 5a). This can be rationalized that upon the disappearance of the SEI layer, the initial graphite edge-sites of C=C–H were replaced by those of C=C–OH as schematically illustrated in the inset of Figure 5a, although the Li intercalation would make the graphite being more reduced. Such graphite surface change is expected to influence the Li intercalation right on the edges of graphite, and consequently affect the ensuing performance of the anode.

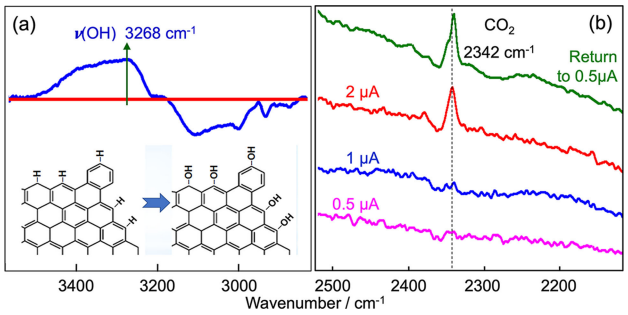

Figure 5. (a) An increase of a band at 3268 cm^{-1} observed in the spectrum taken at 0.25 V, i.e., the top spectrum in Figure 3c. It can be assigned ν(OH) on graphite surface as illustrated in the inset. The reference spectrum was recorded at the OCP that led to the straight horizontal red line as a result of self-normalization (b) Operando ATR-IR spectra acquired at the $LiCoO_2$ cathode during charging with a current of 0.5, 1, 2 μA and a return back to 0.5 μA, respectively.

Investigating the correlation of the formation of =C-OH and the cycle life of LIB is currently ongoing in our lab. On the other hand, it is generally believed that faster charging battery, i.e., using higher current, produces higher cell temperature that can accelerate irreversible chemical reactions in the cell and results in the degradation of the battery performance.[35] Figure 5b shows one of the detrimental effects of faster charging, in which we compare the operando ATR-IR spectra recorded at the $LiCoO_2$ cathode at 60 °C with different charging currents: 0.5 (pink), 1 (blue), 2 μA (red) and a return back to 0.5 μA (green). As can be seen, charging at a higher current, 2 μA, produced a CO_2 band at 2342 cm^{-1} at the cathode,[36] which could be the product of the oxidation of EC and/or DEC caused by the imbalance between the rate of Li-ion leaving the cathode and that of oxidation of Co ions from Co^{3+} to Co^{4+}. Electron deficiency so caused in the $LiCoO_2$ cathode induced high positive overpotential that led to oxidizing electrolyte to CO_2, which is consistent with previous results reported in the literature.[37–45] The formed CO_2 was indeed trapped inside the LIB as evidenced by the green spectrum in which the CO_2 band was still observed even when the charging current was returned to 0.5 μA. However, no CO_2 generation was observed on the anode during the 2-μA charging. To the best of our knowledge, this is the first direct operando spectroscopic observation of CO_2 generation taking place only at the cathode during a battery operation that clarifies the role of charging rate on the gas evolution inside of a LIB.

In conclusions, we reported a novel dual-IR window/electrode operando ATR-IR absorption spectroscopic method for studying batteries chemistry that enables operando IR measurements of both cathode and anode chemistries in the same operating cell quasi-simultaneously without interrupting its operation. The performance of the method was demonstrated by operando IR measurements of a LIB with graphite anode and $LiCoO_2$ cathode and using 1 M $LiPF_6$ dissolved in the mixture of EC:DEC as electrolyte. Our results showed that (1) the SEI layer was formed on both graphite anode and $LiCoO_2$ cathode; (2) the anode SEI layer contained both EC and DEDOHC but the cathode one contained only EC; (3) the DEDOHC was less stable than EC in the anode SEI layer that did not preserve the over-discharging, in great contrast to the cathode SEI layer that did preserve it; (4) over-discharging generated =C–OH groups on the graphite surface; and (5) higher charging current produced CO_2 at the $LiCoO_2$ cathode. Altogether, these observations showcased the investigative advantages of this novel operando IR battery cell in gaining broader insights into battery chemistry.

Acknowledgement

This work was supported by the U.S. Department of Energy, Office of Science, Office of Basic Energy Sciences, Chemical Sciences, Geosciences, and Biosciences Division under Award Number DE-FG02-07ER15895. The authors thank the Georgetown Environment Initiative for an Impact Program Award and Dr. Nathan A. Banek and Professor Michael J. Wagner from George Washington University for enlightening discussions. The sputtering-deposited Cu and Al nanofilm on the Si prisms were manufactured in the Georgetown Nanoscience and Microtechnology Laboratory (GNμLab).

Conflict of Interest

The authors declare no conflict of interest.

Keywords: dual-window operando IR spectroscopy · lithium-ion batteries · over-discharging · solid-electrolyte interphase · total-attenuated reflection IR

[1] M. S. Whittingham, *Che Rev.* **2004**, *104*, 4271–4302.
[2] B. Moradi, G. G. Botte, *J. Appl. Electrochem.* **2016**, *46*, 123–148.
[3] J. B. Goodenough, K.-S. Park, *J. Am. Chem. Soc.* **2013**, *135*, 1167–1176.
[4] J. R. Croy, A. Abouimrane, Z. Zhang, *MRS Bull.* **2014**, *39*, 407–415.
[5] S. Zhang, *Front. Energy Res.* **2013**, *1*, 8.
[6] P. P. R. M. L. Harks, F. M. Mulder, P. H. L. Notten, *J. Power Sources.* **2015**, *288*, 92–105.
[7] J.-T. Li, Z. Y. Zhou, I. Broadwell, S.-G. Sun, *Acc. Chem. Res.* **2012**, *45*, 485–494.
[8] F. Shi, P. N. Ross, G. A. Somorjai, K. Komvopoulos, *J. Phys. Chem. C.* **2017**, *121*, 14476–14483.
[9] C. Marino, A. Boulaoued, J. Fullenwarth, D. Maurin, N. Louvain, J.-L. Bantignies, L. Stievano, L. Monconduit, *J. Phys. Chem. C.* **2017**, *121*, 26598–26606.
[10] A. Vizintin, J. Bitenc, A. Kopač Lautar, K. Pirnat, J. Grdadolnik, J. Stare, A. Randon-Vitanova, R. Dominko, *Nat. Commun.* **2018**, *9*, 661.
[11] J. P. Vivek, N. G. Berry, J. Zou, R. J. Nichols, L. J. Hardwick, *J. Phys. Chem. C.* **2017**, *121*, 19657–19667.
[12] Y.-Q. Bie, J. Horng, Z. Shi, L. Ju, Q. Zhou, A. Zettl, D. Yu, F. Wang, *Nat. Commun.* **2015**, *6*, 1–6.
[13] D. Alves Dalla Corte, G. Caillon, C. Jordy, J.-N. Chazalviel, M. Rosso, F. Ozanam, *Adv. Energy Mater.* **2015**, *6*, 1501768–1501712.
[14] B. M. Koo, D. A. D. Corte, J.-N. Chazalviel, F. Maroun, M. Rosso, F. Ozanam, *Adv. Energy Mater.* **2018**, *8*, 1702568–1702568.
[15] E. G. Sorte, D.-J. Chen, Y. Y. J. Tong, *J. Electrochem. Soc.* **2016**, *163*, H3038-H3042.
[16] F. Shi, H. Zhao, G. Liu, P. N. Ross, G. A. Somorjai, K. Komvopoulos, *J. Phys. Chem. C* **2014**, *118*, 14732–14738.
[17] P. Verma, P. Maire, P. Novák, *Electrochim. Acta.* **2010**, *55*, 6332–6341.
[18] J. E. Owejan, J. P. Owejan, S. C. De Caluwe, J. A. Dura, *Chem. Mater.* **2012**, *24*, 2133–2140.

[19] A. L. Michan, M. Leskes, C. P. Grey, *Chem. Mater.* **2016**, *28*, 385–398.
[20] Y. Li, Y. Li, A. Pei, K. Yan, Y. Sun, C.-L. Wu, L.-M. Joubert, R. Chin, A. L. Koh, Y. Yu, J. Perrino, B. Butz, S. Chu, Y. Cui, *Science.* **2017**, *358*, 506–510.
[21] S. J. An, J. Li, C. Daniel, D. Mohanty, S. Nagpure, D. L. Wood, *Carbon.* **2016**, *105*, 52–76.
[22] H. J. Santner, C. Korepp, M. Winter, J. O. Besenhard, K. C. Möller, *Anal. Bioanal. Chem.* **2004**, *379*, 266–271.
[23] A. Patil, V. Patil, D. Wook Shin, J.-W. Choi, D.-S. Paik, S.-J. Yoon, *MRS Bull.* **2008**, *43*, 1913–1942.
[24] D. Aurbach, B. Markovsky, I. Weissman, E. Levi, Y. Ein-Eli, *Electrochim. Acta.* **1999**, *45*, 67–86.
[25] N. Nitta, F. Wu, J. T. Lee, G. Yushin, *Mater. Today.* **2015**, *18*, 252–264.
[26] E. Peled, D. Golodnitsky, A. Ulus, V. Yufit, *Electrochim. Acta.* **2004**, *50*, 391–395.
[27] K. Naoi, N. Ogihara, Y. Igarashi, A. Kamakura, Y. Kusachi, K. Utsugi, *J. Electrochem. Soc.* **2005**, *152*, A1047–A1053.
[28] E. Peled, D. Golodnitsky, C. Menachem, D. Bar-Tow, *J. Electrochem. Soc.* **1998**, *145*, 3482–3486.
[29] K.-i. Morigaki, A. Ohta, *J. Power Sources.* **1998**, *76*, 159–166.
[30] D. Bar-Tow, E. Peled, L. Burstein, *J. Electrochem. Soc.* **1999**, *146*, 824–832.
[31] M. S. Mubarak, D. G. Peters, *J. Electroanal. Chem.* **1992**, *332*, 127–134.
[32] M. Odziemkowski, D. E. Irish, *J. Electrochem. Soc.* **1993**, *140*, 1546–1555.
[33] E. Fuente, J. A. Menéndez, M. A. Diez, D. Suárez, M. A. Montes-Morán, *J. Phys. Chem. B.* **2003**, *107*, 6350–6359.
[34] C. D. Zangmeister, *Chem. Mater.* **2010**, *22*, 5625–5629.
[35] S. S. Zhang, *J. Power Sources.* **2006**, *161*, 1385–1391.
[36] K. E. Dierenfeldt, *J. Chem. Educ.* **1995**, *72*, 281.
[37] K. H. Lee, E. H. Song, J. Y. Lee, B. H. Jung, H. S. Lim, *J. Power Sources.* **2004**, *132*, 201–205.
[38] M. Metzger, C. Marino, J. Sicklinger, D. Haering, H. A. Gasteiger, *J. Electrochem. Soc.* **2015**, *162*, A1123–A1134.
[39] L. Yang, B. Ravdel, B. L. Lucht, *Electrochem. Solid-State Lett.* **2010**, *13*, A95–A97.
[40] M. Xu, L. Zhou, Y. Dong, Y. Chen, A. Garsuch, B. L. Lucht, *J. Electrochem. Soc.* **2013**, *160*, A2005–A2013.
[41] L. Hu, Z. Zhang, K. Amine, *J. Power Sources.* **2013**, *236*, 175–180.
[42] V. Etacheri, R. Marom, R. Elazari, G. Salitra, D. Aurbach, *Energy Environ. Sci.* **2011**, *4*, 3243–3262.
[43] R. Marom, S. F. Amalraj, N. Leifer, D. Jacob, D. Aurbach, *J. Mater. Chem.* **2011**, *21*, 9938–9954.
[44] N. Takami, T. Ohsaki, H. Hasebe, M. Yamamoto, *J. Electrochem. Soc.* **2002**, *149*, A9–A12.
[45] A. Wuersig, W. Scheifele, P. Novák, *J. Electrochem. Soc.* **2007**, *154*, A449–A454.

Manuscript received: July 26, 2018
Revised manuscript received: October 26, 2018
Version of record online: November 20, 2018